

TeleFMG: A Wearable Force-Myography Device for Natural Teleoperation of Multi-finger Robotic Hands

Alon Mizrahi and Avishai Sintov

Abstract—Teleoperation enables a user to perform tasks from a remote location. Hence, the user can interact with a long-distance environment through the operation of a robotic system. Often, teleoperation is required in order to perform dangerous tasks (e.g., work in disaster zones or in chemical plants) while keeping the user out of harm's way. Nevertheless, common approaches often provide cumbersome and unnatural usage. In this letter, we propose *TeleFMG*, an approach for teleoperation of a multi-finger robotic hand through natural motions of the user's hand. By using a low-cost wearable Force-Myography (FMG) device, musculoskeletal activities on the user's forearm are mapped to hand poses which, in turn, are mimicked by a robotic hand. The mapping is performed by a data-based model that considers spatial positions of the sensors on the forearm along with temporal dependencies of the FMG signals. A set of experiments show the ability of a teleoperator to control a multi-finger hand through intuitive and natural finger motion. Furthermore, transfer to new users is demonstrated.

I. INTRODUCTION

The global outbreak of the COVID-19 presented a great challenge to medical personnel. Medical doctors and nurses were required to balance between the need to provide life-saving treatment to quarantined patients and the necessity to protect themselves from being infected [1]. Personal protective equipment (PPE) cannot fully protect staff and they require to replace them often while shortage is quite common. In addition to infection risks, PPE such as latex gloves and masks is highly polluting with long term environmental impact [2]. These challenges also exist in various other hazardous domains, such as disaster zones, chemical factories, space [3] and deep water [4], where human operators must complete various tasks. Robotic system are the ideal solution to form the required interaction between medical staff and patients with no risk of exposure, or replace human operators in dangerous work.

There have already been many robots working to disinfect hospitals or deliver food and medicine [5]. Similarly, robots are used to inspect hazardous environments [6]. Also, telepresence robots are used for remote meetings with doctors and loved ones [7]. However, active participation of robots, where they fully interact with patients in a clinical setting (e.g., nursing, usage of medical instruments and physical examination) still lacks while they potentially can do much more. Similarly, robots in other hazardous environments are mainly used for inspection and carry equipment, and are limited in actual interaction with the environment. While fully autonomous robots able to manage complex tasks in

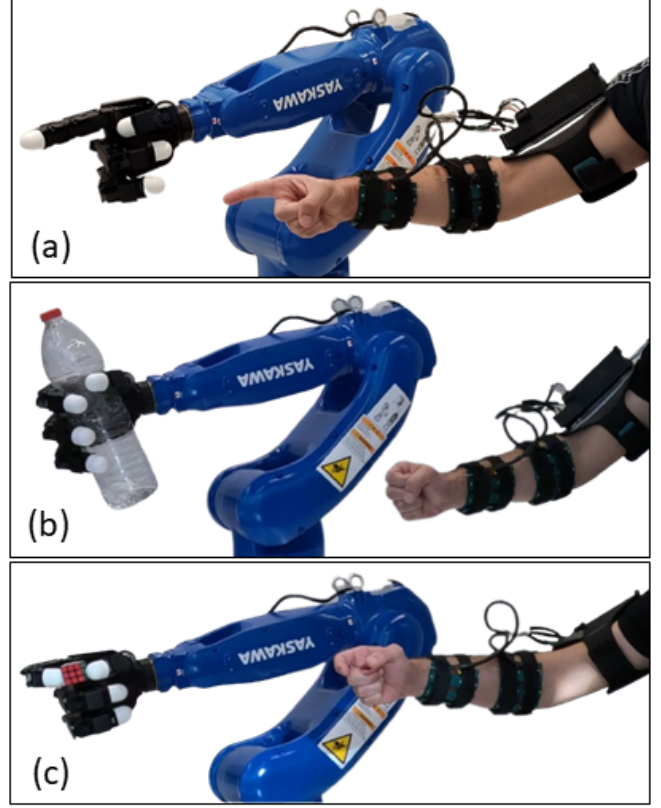


Fig. 1. Teleoperation demonstrations of a multi-finger robotic hand using the TeleFMG device in (a) pointing gesture, (b) whole hand grasping of a bottle and (c) pinch grasping of a small cube.

healthcare and hazardous environments are still some way in the future, human experts must always be in the decision process and have some control. Hence, teleoperation of robots by expert human operators and, particularly, telemedicine (i.e., remote delivery of medical care) [8] by the medical staff are an ideal solution to put them out of harm's way.

In active teleoperation, the state of the human arm and hand are mapped to motion of a robot [9]. Hence, a human operator takes control over robot functions, can drive it through the environment and move a robotic arm in order to perform tasks. A common and simple approach is the use of a game-pad to move the robot [10]. Haptic teleoperation is the use of a specialized joystick or a robotic arm to control another robot along with force feedback in order to simulate the forces that the robot is experiencing [11]. These solutions for teleoperations are usually expensive, non-intuitive, bulky and require much training. More natural

A. Mizrahi and A. Sintov are with the School of Mechanical Engineering, Tel-Aviv University, Israel. E-mail: alonmizrahi2@mail.tau.ac.il, sintov1@tauex.tau.ac.il.

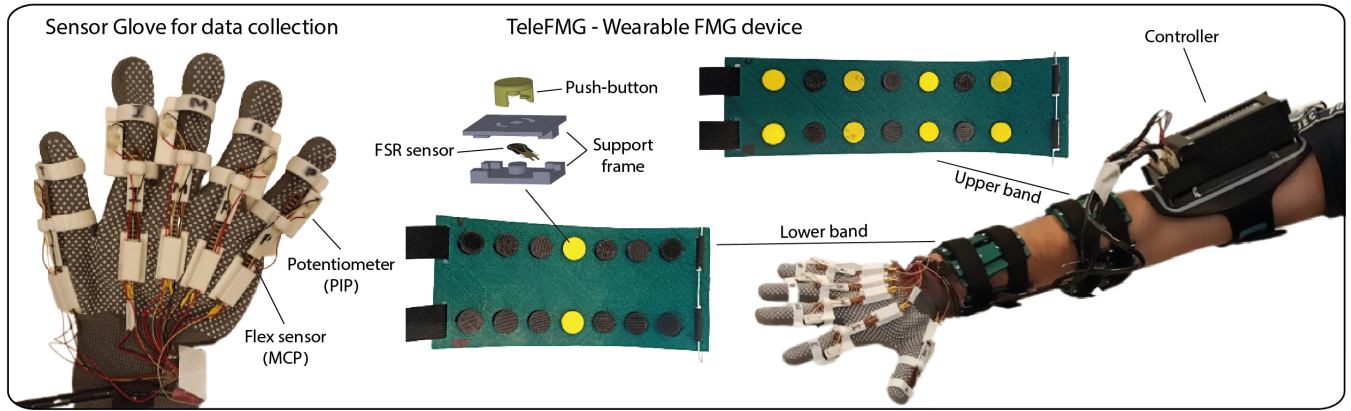


Fig. 2. The TeleFMG system including two bands with 14 FSR sensors each, and the sensor glove for labeling FMG signals with hand poses in the data collection phase.

approaches directly observe the pose of the arm and hand through the use of visual perception or a sensor glove. With vision, an RGB-D camera observes the motion of the user, estimates arm and finger poses through the use of human pose estimation models and moves a robot accordingly [12], [13]. Relying on continuous visual perception limits the performance when visual uncertainty (e.g., poor lighting or shadows) or occlusion may occur. The use of haptic gloves is an alternative through direct measurement of hand poses [14], [15]. While the use of sensor gloves can provide accurate finger pose estimations, they tend to be bulky and expensive while limiting the tactile sensation of the user. Hence, the user must remove them in order to perform other tasks in between teleoperation sessions.

A widely researched approach is to acquire and learn neurological activities through Electro-Myography (EMG) [16]. EMG detects electrical signals generated by muscle tissue. For instance, an EMG was used along with an Inertial Measurement Unit (IMU) in order to teleoperate a robotic arm and anthropomorphic five-finger hand [17]. Similarly, an EMG wrist band was proposed for control of a non-anthropomorphic robotic gripper [18]. A different work combined EMG with a haptic device to control a mobile robot [19]. EMG, however, usually requires extensive training along with expensive and highly sizable equipment. Also, EMG accuracy may be compromised by electrode placement, sweat and crosstalk [20]. Force-Myography (FMG), on the other hand, is an easier alternative to sense the state of a human arm [21]. FMG signals were shown to be simple to acquire with a relatively high-accuracy. Consequently, FMG was used in data-based classification of hand gestures [22], [23] and rehabilitation studies [24]. Comparative studies have shown that FMG is less sensitive to positioning variations, does not require direct contact with the skin, and significantly outperforms EMG's accuracy [25], [26]. Previous work by the authors have shown that FMG can be used to recognize objects grasped by the human hand [27] and can generalize to various new users [28]. With such information, a robot in a Human-Robot Collaboration (HRC) scenario can identify a grasped tool, infer about the intended task and act to assist.

In order to be appealing, teleoperation and interaction with

a robotic system must be natural, intuitive and ergonomic. Wearable FMG offers such qualities with easy-to-use and low cost hardware. While FMG has been previously used in a wide variety of classification tasks, it was never explored in the context of finger pose estimation for teleoperation. In this work, we explore the ability of FMG to accurately map FMG signals to the physical state of the human hand, i.e., estimate finger joint angles. We introduce the *TeleFMG* system. TeleFMG is a wearable FMG device worn on the user's forearm, similar to the one proposed in [27], and used alongside with a data-based model in order to estimate the pose of the human fingers. With the benchmarking of various neural-network models, we observe the required data for accurate finger pose estimation and teleoperation of a robotic system. We investigate the accuracy of a model trained with data collected from one user and the effort required to transfer it to new users.

In addition to accuracy evaluation, we are also interested in the ability of the model to successfully transfer tasks from the user to the robotic hand. Such tasks include hand gestures, whole hand grasping and pinching (Figure 1). With such capability, a user can remotely control a multi-finger hand. While not in the scope of this work, the motion of a robotic arm equipped with the hand can be performed by including an IMU on the wearable system in order to track and approximate motion [29]. Nevertheless, the operation of a dexterous robotic hand with a multitude of degrees of freedom is more complex and is the focus of our work.

II. METHOD

A. FMG wearable device

Previous work by the authors has proposed a low-cost wearable FMG device in the context of HRC [27]. Based on the design, an advanced prototype is developed and fabricated. The device, seen in Figure 2, is composed of 28 Force-Sensitive Resistors (FSR), short-tail model FSR-400 by Interlink Electronics. FSR sensors are composed of thin sheets of polymer that alter their electrical resistance in response to the amount of pressure applied to their surface. The sensors are arranged on two bands, upper and lower forearm bands, each having 14 FSR sensors equally spaced

in two rows. The bands are fabricated by 3D printing with an elastic polymer (Thermoplastic elastomer). Hence, they are flexible, light-weight and allow unrestricted movement of the entire arm. To ensure compliant skin press on the FSR sensors, each sensor is covered by a push-button mechanism. The button includes an inner bulge that presses on the FSR even if the surface of the button is not parallel to the FSR. This enables adaptation on the uneven surface of the user's forearm with continuous contact.

All FSR sensors are connected to a Teensy 4.1 micro-controller. Since the Teensy has only 18 analog channels, each two sensors of the 28 ones are connected to the same analog input in the Teensy through a voltage divider of $4.7k\Omega$ resistor. Using a transistor-based (mini MOSFET) switching system, the Teensy is able cyclically sample different sets of sensors in a frequency of up to 40 Hz and transfer to a computing unit via cable. While not utilized in this work, a Bluetooth component was included and can handle wireless transfer of data in real-time.

B. Sensor Glove

The wearable device measures FMG signals from the forearm in order to map them to finger poses. A labeling system is required for recording the state of the hand. Hence, a hand labeling device based on a glove was developed. The device is composed of a cloth glove with five 2.2" SEN-10264 ROHS flex sensors and five potentiometers model PT15NH05-103A2020-S by Amphenol Piher. The flex sensors bridge the back of the hand and fingers over the knuckles, and measure the angle $\theta_{MCP,i}$ of the Metacarpophalangeal (MCP) joints where $i = \{1, \dots, 5\}$ is the index of the finger. Similarly, the potentiometers measure the angle $\theta_{PIP,i}$ of the Proximal Interphalangeal (PIP) joints. While the potentiometers straight-forwardly provide joint angle, the flex sensors were calibrated to map deflection to angles. In total, the sensors measure ten finger angles on the hand. In this work, we do not consider abduction and adduction motions of the fingers. The sensors are connected to the glove using 3D-printed flanges and stitches. During data collection, the labeling system is connected to a main computer along with the FMG device to allow synchronous stream of data.

C. Problem Formulation

With the above wearable and labeling hardware, we aim to map FMG sensing to finger pose of the human hand. Let $\mathbf{x} \in \mathbb{R}^{28}$ be the observable state of the musculoskeletal system measured by the 28 FSR sensors on the FMG device in contact with the forearm. Similarly, the state of the hand $\mathbf{q} \in \mathbb{R}^{10}$ is the set of 10 finger joint angles where $\mathbf{q} = \{\theta_{MCP,1}, \theta_{PIP,1}, \dots, \theta_{MCP,5}, \theta_{PIP,5}\}$. The angles are zero when the fingers are fully extended. We search for a model f which maps FMG signals to the pose of the hand. Since an analytical model for such map cannot be acquired, we search for a robust and multi-user data-based model. With such a model, a robotic hand can mimic the motion of the human hand in real-time.

D. Data Collection

Training data is collected by recording FMG states through the wearable device and synchronously labeling them with hand states using the sensor glove. With a stream rate of 33 Hz, each FMG sample \mathbf{x}_i is recorded along with its corresponding hand state \mathbf{q}_i . Data is collected on a single participant in n sessions. Before each session, the device is taken off of the forearm and re-positioned in order to collect data with positional uncertainty. In the beginning of the session and right after the FMG device was positioned on the forearm, a set of samples was taken while the participant relaxed arm muscles. The mean vector \mathbf{x}_o of these samples is considered as the session baseline and is subtracted from any sample recorded in the session, i.e., $\tilde{\mathbf{x}}_i = \mathbf{x}_i - \mathbf{x}_o$. Such subtraction compensates for non-equal and non-uniform tightening of the device between sessions.

During a session, which included m recorded samples, the participant conducted various random motions of the fingers. Since the musculoskeletal system can vary with the same finger pose but with motion of the arm and wrist, data is collected while also randomly manipulating the wrist and arm in the workspace. Sessions also included task performing such as gripping of various objects and common gestures. The resulting training data is a set of $N = mn$ labeled FMG measurements $\mathcal{P} = \{(\tilde{\mathbf{x}}_1, \mathbf{q}_1), \dots, (\tilde{\mathbf{x}}_N, \mathbf{q}_N)\}$. A similar dataset was collected for testing trained models in independent collection sessions.

E. Data-based Model

The presented problem requires supervised learning over dataset \mathcal{P} by means of regression. One may train a Fully-Connected Neural-Network (FC-NN) to directly map a single FMG signal $\tilde{\mathbf{x}}_i$ to the corresponding pose \mathbf{q}_i of the hand. However, it is hypothesized that temporal sequence reading of FMG signals would provide more accurate pose estimations. Let $\mathcal{S}_H \subset \mathbb{R}^{28} \times \dots \times \mathbb{R}^{28}$ be the product space of the observable FMG space over H sequential measurements. In a pre-processing step, dataset \mathcal{P} is modified to include sequences of H FMG signals. That is, a temporal FMG sequence of length H at time t

$$\mathcal{S}_t = \{\tilde{\mathbf{x}}_{t-H}, \dots, \tilde{\mathbf{x}}_{t-1}, \tilde{\mathbf{x}}_t\} \in \mathcal{S}_H \quad (1)$$

is extracted from \mathcal{P} and labeled with the corresponding hand pose \mathbf{q}_t . Hence, a new dataset $\mathcal{P}' = \{(\mathcal{S}_1, \mathbf{q}_1), \dots, (\mathcal{S}_{N-H}, \mathbf{q}_{N-H})\}$ is used to train a temporal-based model. We hypothesise that the system is govern by a map $f : \mathcal{S}_H \rightarrow \mathbb{R}^{10}$. Hence, temporal measurements from the FMG device can be mapped to the state of the hand at time t through

$$\mathbf{q}_t = f(\mathcal{S}_t). \quad (2)$$

Training a sequential model for (2) can be done using the Long Short-Term Memory (LSTM). LSTM is a class of Recurrent Neural-Networks (RNN) aimed to learn sequential data [30]. LSTM is able to selectively retain or discard information from previous time steps making it well-suited for long-term dependencies. However, LSTM models can

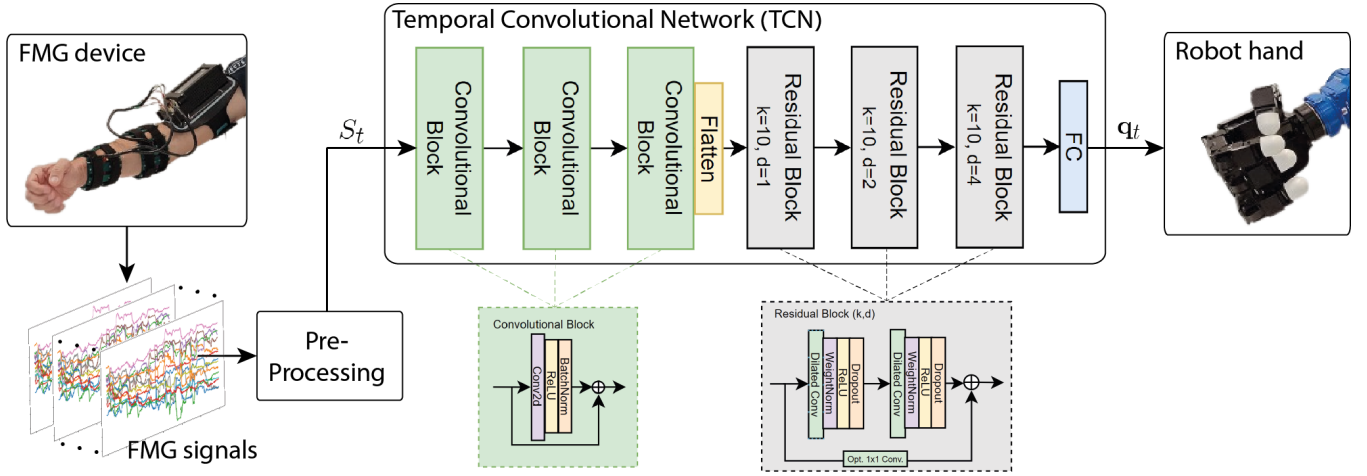


Fig. 3. An illustration of the TCN model which acquires spatio-temporal FMG signals and maps them to the pose of the human hand. The pose is mimicked by a robotic hand.

be computationally expensive and slow to train, particularly for longer sequences [31]. Also, LSTM cannot preserve the relative positions between sensors on the FMG device. Convolutional Neural-Networks (CNN) are commonly used to learn image data and any tabular data. Hence, it is possible to formulate an array where the components are organized in the formation of the FSR sensors on the FMG device. A single channel array is then fed into the convolutional layers of the CNN. Nevertheless, such form cannot take temporal dependencies into account. In other words, it would be beneficial for a model to observe the spatial and temporal relations in the FMG signals, i.e., we require a spatio-temporal model [32].

Each FMG signal vector $\tilde{\mathbf{x}}_{t-i} \in S_t$ is reshaped to a matrix U_{t-i} of size 4×7 . In such form, a component $u_{t-i}^{(a,b)}$ in U_{t-i} denotes the FMG signal in row a and column b of the FMG device. Hence, matrix U_{t-i} provides a spatial representation of the FMG measurement on the forearm. Consequently, a reformulated sequence

$$S_t = \{U_{t-H}, \dots, U_{t-1}, U_t\} \quad (3)$$

is a spatio-temporal representation of the data. To formulate a spatio-temporal model, we use a Temporal Convolutional Network (TCN) [33]. TCN is a type of NN that uses convolutional layers to process sequential data. The convolutional layers extract significant features from the data. By using dilated convolutions, the TCN is able to capture long-term dependencies in a computationally efficient manner, making it a popular and efficient choice for temporal prediction tasks.

Our proposed TCN architecture is illustrated in Figure 3. Each matrix $U_{t-H} \in S_t$ undergoes three convolutional layers to extract meaningful features. Each convolution layer includes a ReLU activation function, batch normalization and a skip connection. After passing through the convolutional layers, the H outputted matrices of size 7×7 are flattened and treated as a sequence of H vectors. These vectors are then fed into three residual blocks which employ 1D dilated convolutions. A dilated convolutional layer allows the kernel of size k to observe a wider area of the input without

having to increase its size, enabling to analyze the temporal changes in the features over time. This is done by skipping $d - 1$ elements between the kernel elements where d is the dilation rate. The kernels of all three residual blocks have size $k = 10$ while dilation rate increases to $d = 1, 2, 4$ between layers. The proposed model was trained with \mathcal{P}' while adding Gaussian noise for robustness.

F. Real time work

Given the trained TCN model, estimated poses \mathbf{q}_t of the human hand are to be mimicked by a multi-finger robotic hand in a teleoperation setup. Anthropomorphic robot hands usually have four- (e.g., Allegro hand) or five- (e.g., Shadow [34] and DLR [35] hands) fingers. In the case of a five-finger robotic hand, the finger joint angles are directly mapped to the joints of the robotic hand. When considering a four-finger robotic hand, the joint angle estimations of the little (pinky) finger are disregarded as it minimally degrades the functionality of the hand.

For each finger on the users hand, the MCP and PIP angles are estimated with FMG signals as described above. Then, they are directly mapped to the corresponding joints of the robotic hand. However, the Distal Interphalangeal (DIP) joints at the tips of the user's fingers are not measured. Yet, the human hand is known to have coupled movements termed *synergies* [36]. A common representation of the synergies between the PIP and DIP of each finger is $\theta_{\text{DIP},i} = \frac{2}{3}\theta_{\text{PIP},i}$ [9], [37]. Such ratio was used in our implementation in order to determine the DIP angles of a robotic hand based on estimation of the PIP ones on the users hand.

III. EXPERIMENTS AND RESULTS

In this section, we test and analyze the accuracy of a trained model and the ability of a user to teleoperate a robotic hand through FMG. Videos of data collection and experiments can be seen in the supplementary material.

A. Database

Dataset \mathcal{P} was collected from one participant as described in Section II-D using the FMG device and labeling glove.

The collection included $n = 15$ sessions with $m = 25,530$ recorded samples yielding a total of $N = 382,950$ training samples. The FMG device was taken off between sessions and reapplied in slightly altered locations. In addition, a test set of 105,000 samples was recorded in 5 separate sessions not included in the training. Snapshots from a collection session are seen in Figure 4.

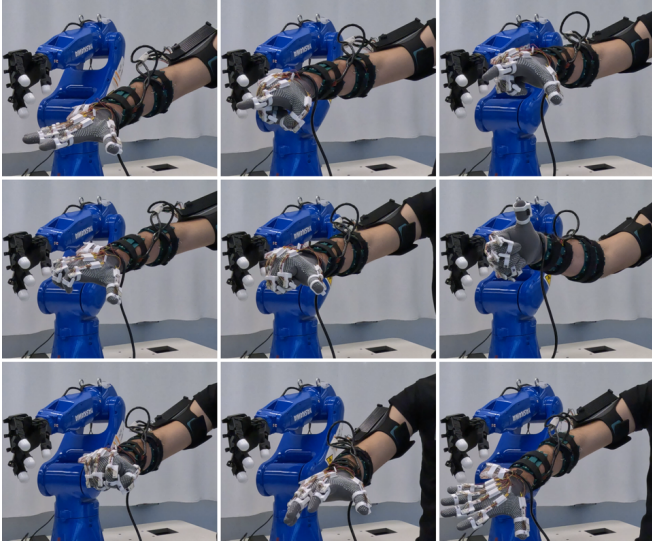


Fig. 4. Snapshots of data collection using the FMG device and the labeling glove in various hand poses.

B. Model Evaluation

We analyzed the performance of various deep learning models trained on dataset \mathcal{P} . The use of TCN as discussed in Section II-E is benchmarked with other models including: FC-NN outputting ten joint angles; five FC-NN ($5 \times \text{FC-NN}$), one for each finger; LSTM; and CNN. For FC-NN and $5 \times \text{FC-NN}$, the hand pose is estimated solely based on an instantaneous FMG measurement, i.e., $\mathbf{q}_t = f(\mathbf{x}_t)$. Similarly, the CNN considers instantaneous FMG measurements formulated as arrays based on sensor locations on the device. On the other hand, LSTM can consider temporal sequences of FMG measurement as in (1). Hence, a sequence S_t of flattened FMG signals at time t is directly fed into the model to predict \mathbf{q}_t . For the TCN, the data was modified to formulate matrices as in (3) prior to training and testing. Hyper-parameters of all models were optimized to provide best results.

TABLE I
ESTIMATION ACCURACY FOR DIFFERENT MODELS

Model	Angle error ($^\circ$)
$5 \times \text{FC-NN}$	14.60 ± 0.80
FC-NN	13.60 ± 2.05
CNN	15.61 ± 3.37
LSTM	13.38 ± 2.51
TCN	9.76 ± 1.65

TABLE II
ANGLE ESTIMATION ERRORS ($^\circ$) FOR EACH FINGER AND JOINT

	Thumb	Index	Middle	Ring	Little
MCP	12.03	9.92	9.19	8.65	8.11
PIP	12.81	11.6	8.54	8.31	8.48

Table I summarizes the mean angle error over the test data and for all five models. First, momentary observation of FMG signals with FC-NN exhibits poor results. Solely re-structuring the data to learn spatial dependencies with a CNN does not provide additional accuracy. Similarly, only observing temporal dependencies in the data with an LSTM does not provide additional accuracy improvement. By including spatial representation of the FMG data to the temporal sequencing, TCN exhibits superior results. Table II presents the mean errors when individually estimating each finger joint using the TCN model. The larger errors originate from the thumb where the Carpometacarpal (CMC) joint is not modeled and provides some uncertainties. Figure 5 shows an example of real-time estimation of finger motions using the FMG device. The results show the ability to estimate hand poses based on FMG signals.

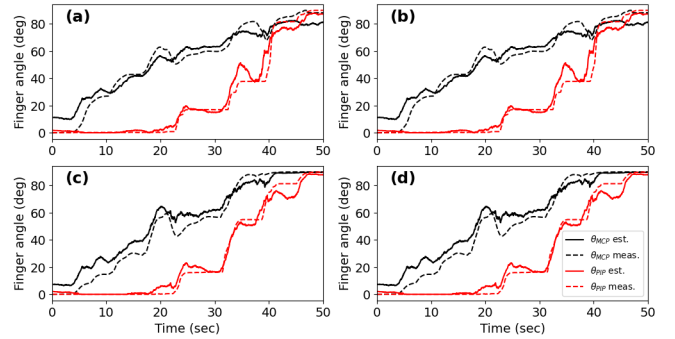


Fig. 5. Example of real-time estimation of finger joint angles based on FMG for (a) thumb, (b) index finger, (c) middle finger and (d) ring finger.

C. Teleoperation evaluation

With the trained model, we wish to evaluate TeleFMG on a robotic hand. Hence, we experiment with the four-finger Allegro hand by Wonik Robotics. The Allegro is a fully-actuated hand comprised of 16 actuators, four in each finger. Three actuators on each finger control the MCP, PIP and DIP while the fourth actuate abduction and adduction motions. The latter is not used in this work and manually set to a constant value.

TeleFMG is first tested for teleoperation of several hand gestures including: open hand, closed hand, pointing with the index finger, thumbs-up, and a two-finger V-sign with the index and middle fingers. Then, we test the teleoperation for performing five tasks of interaction with objects including: whole hand grasp of a ball and a bottle, grasp of a thin elongated object such as a screwdriver and a brush handle, pinch grasping of small objects such as an ATM card, cube and rubber duck, and lifting bags with four fingers. We first

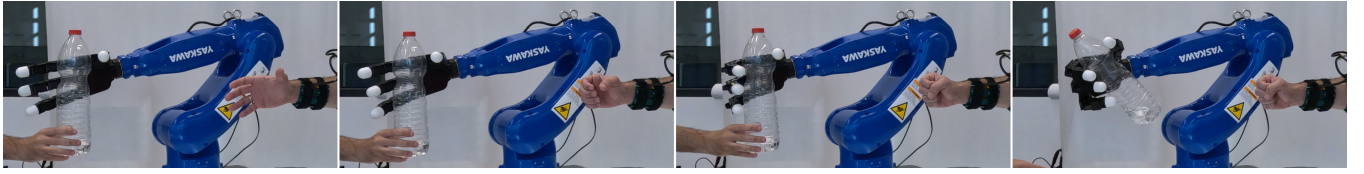


Fig. 6. Snapshots of the 4-finger Allegro hand grasping a bottle using TeleFMG.



Fig. 7. Snapshots of the 4-finger Allegro hand pinch grasping an ATM card using TeleFMG.

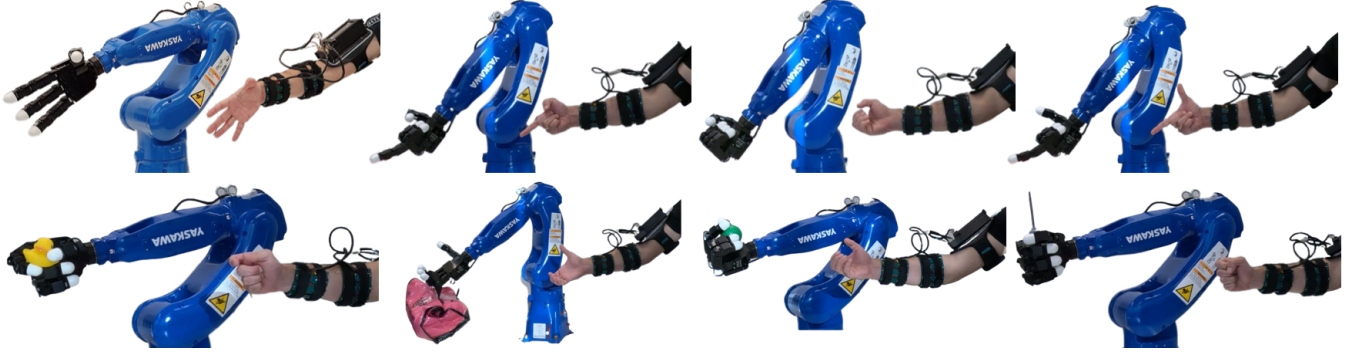


Fig. 8. Snapshots of the 4-finger Allegro hand mimicking the motion of the user through TeleFMG in (top row) gestures and (bottom row) grasping various objects including (left to right) rubber duck, bag, ball and screwdriver.

test the success rate of mimicking the gestures and actions of the participant whom contributed the training data.

Table III presents the success rate out of 20 attempts. Overall, all tasks were performed with high success rate. Tasks that involve the thumb such as thumbs-up and pinch grasping failed slightly more often due to more inaccuracies of the thumb as discussed previously. This can be coped by modeling of the CMC joint in future work. Teleoperation snapshots of real-time whole hand grasping of a bottle and pinch grasping of an ATM card can be seen in Figures 6 and 7, respectively. Similarly, Figure 8 shows teleoperation demonstration of various gestures and object grasping. We note that some lagging between user and robot motions occur due to communication limitations of the hardware.

D. TeleFMG for new users

The TeleFMG evaluated above was trained and tested on a single participant. We now wish to test the ability of the trained model to generalize to novel users not included in the training. Four new test participants were used for testing teleoperation while having a variety of forearm dimensions. Table IV provides a list of anthropometric measures (i.e., forearm length (FL), lower forearm circumference (LFC) and upper forearm circumference (UFC)) for the four participants and the total success rate for performing the tasks listed in Table III. While relatively low, the results show an ability to transfer the model to different users. Note that the device did

TABLE III
TELEOPERATION SUCCESS RATE OF GESTURES AND ACTIONS

	Task	Success rate (%)
Gestures	Open hand	100
	Close hand	100
	Index-point	95
	Thumbs-up	80
	2-Fingers	90
Actions	Grasp ball	100
	Grasp bottle	100
	Grasp pole	100
	Pinch grasp	85
	4-finger lift	95
Total		94.5

not fit well to User 3 due to a smaller forearm circumference resulting in lower success rate.

To improve generalization abilities, one can collect training data from various users as in [28]. Another approach, tested here, is to fine-tune the TCN model with a limited amount of training data from the new user. Given a user, we fine-tune the model with a learning rate of 10^{-5} and 8 epochs with some data collected from the user using the sensor glove. Figure 9 shows success rate results after fine-tuning the model for users 1 and 2 with regards to the number of samples collected from the user. Results show that with new data of up to 5% of the size of the original training

TABLE IV
TELEOPERATION SUCCESS RATE FOR NEW USERS

User	Gender	FL (cm)	FLC (cm)	UFC (cm)	Success rate (%)
1	M	27	17	25	66
2	M	28	18	27	60
3	F	23	16.5	21	51
4	M	30	19.5	29	61

data, the model was tuned to 91% and 86% for users 1 and 2, respectively. Such data collection for fine-tuning takes approximately 10 minutes. Figure 10 shows a demonstration of User 1 performing a pointing gesture after the fine-tuning of the model.

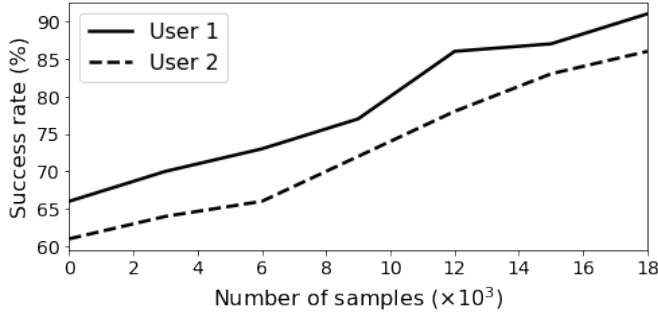


Fig. 9. Teleoperation total task success rate in model fine-tuning for new users 1 and 2 with regards to the number of new samples collected from the users.

E. Feature Importance

We now explore the importance of the FSR sensors on joint angle prediction accuracy. Permutation feature importance is a common method to evaluate the impact of each feature in a model [38]. We measure the increase in the prediction error after permuting the values of each single sensor in the test data separately. The score is the error increase resulting from the permutation of a sensor's values and is computed according to

$$E_i = \frac{e_i - e}{e} \times 100\%, \quad (4)$$

where e is the mean error of the non-permuted model and e_i is the mean error when feature i is permuted. Sensor placements and sensor importance heatmap are illustrated in Figure 11. Table V provides the numeric values of the

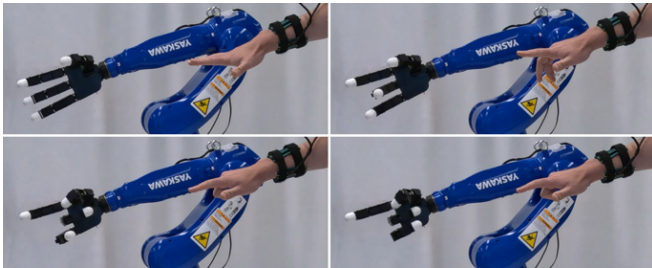


Fig. 10. Demonstration of User 2 teleoperating a pointing gesture after fine-tuning the model.

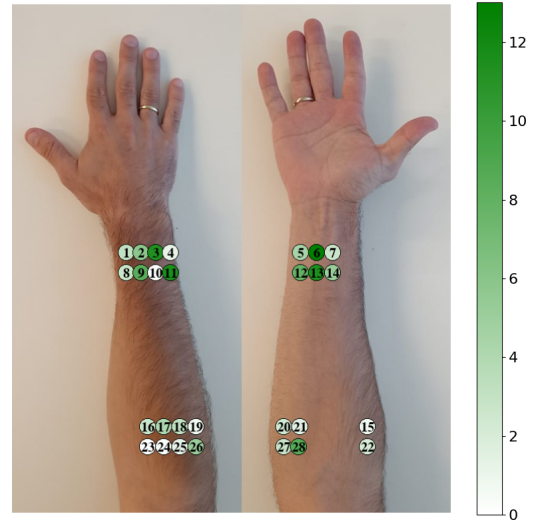


Fig. 11. Illustration of the sensor locations and feature importance scores of the FSR sensors on the FMG device.

TABLE V
FEATURE IMPORTANCE SCORES OF THE FSR SENSORS
ON THE FMG DEVICE

Sensor index	Importance score [%]	Sensor index	Importance score [%]
1	3.180	15	0.813
2	5.816	16	2.706
3	11.386	17	4.063
4	1.173	18	3.123
5	4.387	19	0.741
6	13.013	20	2.287
7	2.644	21	1.433
8	2.746	22	2.016
9	8.485	23	0.117
10	0.254	24	0.322
11	11.605	25	1.182
12	7.841	26	5.113
13	11.583	27	2.824
14	5.083	28	8.643

feature importance. Similar to previous results in [28], the relative errors indicate high dependence on the lower forearm sensors. Nevertheless, most sensors along the arm contribute to pose estimation accuracy.

IV. CONCLUSIONS

In this paper, we have shown the ability of Force-Myography (FMG) on the forearm to estimate the pose of the human hand. Hence, the proposed TeleFMG enables teleoperation of robotic hands through natural motions of the human hand. In TeleFMG, a wearable FMG device is used to measure musculoskeletal activities on the forearm and map them, using a data-based model, to corresponding poses of the hand. It has been shown that a data-based model that maintains the relative spatial positions of the sensors on the forearm along with consideration of temporal dependencies provides best accuracy. Furthermore, a set of teleoperation experiments shows the ability to naturally

command a multi-finger robotic hand to mimic gestures and grasping tasks. Future work to advance TeleFMG may include an IMU for telemanipulation of an entire arm in addition to the hand. Furthermore, the addition of haptic actuators on the device can provide tactile sensation to the user upon contact of a robotic finger and applied forces. For a complete system, virtual reality goggles can be included for a sense of presence.

REFERENCES

- [1] S. R. Razu, T. Yasmin, T. B. Arif, M. S. Islam, S. M. S. Islam, H. A. Gesesew, and P. Ward, "Challenges faced by healthcare professionals during the covid-19 pandemic: A qualitative inquiry from bangladesh," *Frontiers in Public Health*, vol. 9, 2021.
- [2] G. Kannan, B. Mghili, G. E. D. la Torre, P. Kolandhasamy, M. Machendiranathan, M. V. Rajeswari, and A. Saravanakumar, "Personal protective equipment (ppe) pollution driven by covid-19 pandemic in marina beach, the longest urban beach in asia: Abundance, distribution, and analytical characterization," *Marine Pollution Bulletin*, vol. 186, p. 114476, 2023.
- [3] H. Chen, P. Huang, and Z. Liu, "Mode switching-based symmetric predictive control mechanism for networked teleoperation space robot system," *IEEE/ASME Trans. on Mechat.*, vol. 24, no. 6, pp. 2706–2717, 2019.
- [4] S. Sivčev, J. Coleman, E. Omerdić, G. Dooly, and D. Toal, "Underwater manipulators: A review," *Ocean Engineering*, vol. 163, pp. 431–450, 2018.
- [5] S. Ozturkcan and E. Merdin-Uygur, "Humanoid service robots: The future of healthcare?" *Journal of Information Technology Teaching Cases*, vol. 12, no. 2, pp. 163–169, 2022.
- [6] M. Fisher, R. C. Cardoso, E. C. Collins, C. Dadswell, L. A. Dennis, C. Dixon, M. Farrell, A. Ferrando, X. Huang, M. Jump, G. Kourtis, A. Lisitsa, M. Luckcuck, S. Luo, V. Page, F. Papacchini, and M. Webster, "An overview of verification and validation challenges for inspection robots," *Robotics*, vol. 10, no. 2, 2021.
- [7] L. Hung, G. Hu, J. Wong, H. Ren, N. Ahmed, A. Hussein, E. Young, A. Berndt, J. Mann, R. Corepal, and L. Wong, "Telepresence robots in long-term care settings in british columbia during the covid-19 pandemic: Analyzing the experiences of residents and family members," *Gerontology and Geriatric Medicine*, vol. 9, 2023.
- [8] J. Laigaard, T. U. Fredskild, G. L. Fojecki, and F. Hu, "Telepresence robots at the urology and emergency department: A pilot study assessing patients' and healthcare workers' satisfaction," *Int. J. Telemedicine Appl.*, 2022.
- [9] R. Li, H. Wang, and Z. Liu, "Survey on mapping human hand motion to robotic hands for teleoperation," *IEEE Transactions on Circuits and Systems for Video Technology*, vol. 32, no. 5, pp. 2647–2665, 2022.
- [10] A. García, J. E. Solanes, A. Muñoz, L. Gracia, and J. Tornero, "Augmented reality-based interface for bimanual robot teleoperation," *Applied Sciences*, vol. 12, no. 9, 2022.
- [11] J. Singh, A. R. Srinivasan, G. Neumann, and A. Kucukyilmaz, "Haptic-guided teleoperation of a 7-dof collaborative robot arm with an identical twin master," *IEEE Transactions on Haptics*, vol. 13, no. 1, pp. 246–252, 2020.
- [12] A. Handa, K. Van Wyk, W. Yang, J. Liang, Y.-W. Chao, Q. Wan, S. Birchfield, N. Ratliff, and D. Fox, "Dexpilot: Vision-based teleoperation of dexterous robotic hand-arm system," in *IEEE International Conference on Robotics and Automation (ICRA)*, 2020.
- [13] Q. Gao, Z. Ju, Y. Chen, Q. Wang, and C. Chi, "An efficient rgb-d hand gesture detection framework for dexterous robot hand-arm teleoperation system," *IEEE Transactions on Human-Machine Systems*, vol. 53, no. 1, pp. 13–23, 2023.
- [14] P. Weber, E. Rueckert, R. Calandra, J. Peters, and P. Beckerle, "A low-cost sensor glove with vibrotactile feedback and multiple finger joint and hand motion sensing for human-robot interaction," in *IEEE International Symposium on Robot and Human Interactive Communication (RO-MAN)*, 2016, pp. 99–104.
- [15] "Haptx gloves," <https://haptx.com/>.
- [16] L. Bi, A. G. Feleke, and C. Guan, "A review on EMG-based motor intention prediction of continuous human upper limb motion for human-robot collaboration," *Biomedical Signal Processing and Control*, vol. 51, pp. 113 – 127, 2019.
- [17] M. T. Wolf, C. Assad, M. T. Vernacchia, J. Fromm, and H. L. Jethani, "Gesture-based robot control with variable autonomy from the jpl biosleeve," in *IEEE International Conference on Robotics and Automation*, 2013, pp. 1160–1165.
- [18] C. Meeker and M. Ciocarlie, "Emg-controlled non-anthropomorphic hand teleoperation using a continuous teleoperation subspace," in *IEEE International Conference on Robotics and Automation (ICRA)*, 2019, pp. 1576–1582.
- [19] J. Luo, Z. Lin, Y. Li, and C. Yang, "A teleoperation framework for mobile robots based on shared control," *IEEE Robotics and Automation Letters*, vol. 5, no. 2, pp. 377–384, 2020.
- [20] E. Fujiwara, Y. T. Wu, C. K. Suzuki, D. T. G. de Andrade, A. R. Neto, and E. Rohmer, "Optical fiber force myography sensor for applications in prosthetic hand control," in *2018 IEEE 15th International Workshop on Advanced Motion Control (AMC)*. IEEE, 2018, pp. 342–347.
- [21] O. Amft, H. Junker, P. Lukowicz, G. Troster, and C. Schuster, "Sensing muscle activities with body-worn sensors," in *Int. Workshop on Wearable and Implantable Body Sensor Networks*, 2006, pp. 4–pp.
- [22] G. Ogris, M. Kreil, and P. Lukowicz, "Using fsr based muscle activity monitoring to recognize manipulative arm gestures," in *IEEE international symposium on wearable computers*, 2007, pp. 45–48.
- [23] N. Li, D. Yang, L. Jiang, H. Liu, and H. Cai, "Combined use of FSR sensor array and SVM classifier for finger motion recognition based on pressure distribution map," *Journal of Bionic Engineering*, vol. 9, no. 1, pp. 39–47, 2012.
- [24] H. K. Yap, A. Mao, J. C. H. Goh, and C. Yeow, "Design of a wearable FMG sensing system for user intent detection during hand rehabilitation with a soft robotic glove," in *IEEE Int. Conf. on Biomedical Rob. and Biomech.*, 2016, pp. 781–786.
- [25] X. Jiang, L.-K. Merhi, Z. G. Xiao, and C. Menon, "Exploration of force myography and surface electromyography in hand gesture classification," *Med. Engineering & Physics*, vol. 41, pp. 63–73, 2017.
- [26] A. Belyea, K. Englehart, and E. Scheme, "FMG versus EMG: A comparison of usability for real-time pattern recognition based control," *IEEE Trans. on Biomed. Eng.*, vol. 66, no. 11, pp. 3098–3104, 2019.
- [27] N. D. Kahanowich and A. Sintov, "Robust classification of grasped objects in intuitive human-robot collaboration using a wearable force-myography device," *IEEE Robotics and Automation Letters*, vol. 6, no. 2, pp. 1192–1199, 2021.
- [28] E. Bamani, N. D. Kahanowich, I. Ben-David, and A. Sintov, "Robust multi-user in-hand object recognition in human-robot collaboration using a wearable force-myography device," *IEEE Robotics and Automation Letters*, vol. 7, no. 1, pp. 104–111, 2022.
- [29] S. Li, J. Jiang, P. Ruppel, H. Liang, X. Ma, N. Hendrich, F. Sun, and J. Zhang, "A mobile robot hand-arm teleoperation system by vision and imu," in *IEEE/RSJ International Conference on Intelligent Robots and Systems (IROS)*, 2020, p. 10900–10906.
- [30] Y. Yu, X. Si, C. Hu, and J. Zhang, "A Review of Recurrent Neural Networks: LSTM Cells and Network Architectures," *Neural Computation*, vol. 31, no. 7, pp. 1235–1270, 07 2019.
- [31] A. Orvieto, S. L. Smith, A. Gu, A. Fernando, C. Gulcehre, R. Pascanu, and S. De, "Resurrecting recurrent neural networks for long sequences," *ArXiv*, vol. abs/2303.06349, 2023.
- [32] S. Wang, J. Cao, and P. S. Yu, "Deep learning for spatio-temporal data mining: A survey," *IEEE Transactions on Knowledge and Data Engineering*, vol. 34, no. 8, pp. 3681–3700, 2022.
- [33] S. Bai, J. Z. Kolter, and V. Koltun, "An empirical evaluation of generic convolutional and recurrent networks for sequence modeling," in *Conference on Robotics Research*, vol. abs/1803.01271.
- [34] P. Tuffield and H. Elias, "The shadow robot mimics human actions," *Industrial Robot: An Int. Journal*, vol. 30, no. 1, pp. 56–60, 2003.
- [35] J. Butterfass, M. Grebenstein, H. Liu, and G. Hirzinger, "Dlr-hand ii: next generation of a dextrous robot hand," in *IEEE International Conference on Robotics and Automation*, vol. 1, 2001, pp. 109–114.
- [36] N. J. Jarque-Bou, A. Scano, M. Atzori, and H. Müller, "Kinematic synergies of hand grasps: a comprehensive study on a large publicly available dataset," *J. of NeuroEng. and Rehabilitation*, vol. 16, 2019.
- [37] F. C. Chen, A. Favetto, M. Mousavi, E. Ambrosio, S. Appendino, D. Manfredi, F. Pescarmona, G. Calafiore, and B. Bona, *Human Hand: Kinematics, Statics, and Dynamics*, 2011.
- [38] J. Yang, K.-Q. Shen, C. Ong, and X.-P. Li, "Feature selection for mlp neural network: The use of random permutation of probabilistic outputs," *IEEE Trans. on Neural Net.*, vol. 20, pp. 1911 – 1922, 2010.